Journal of Power Sources 229 (2013) 258–264

Contents lists available at SciVerse ScienceDirect

Journal of Power Sources

journal homepage: www.elsevier.com/locate/jpowsour

Synthesis and characterization of nanoparticulate $La_{0.6}Sr_{0.4}CoO_{3-\delta}$ cathodes for thin-film solid oxide fuel cells

Cahit Benel [a,b,c,*], Azad J. Darbandi [a,b], Ruzica Djenadic [a,b,d], Anna Evans [e], René Tölke [e], Michel Prestat [e], Horst Hahn [a,b]

[a] Institute for Nanotechnology, Karlsruhe Institute of Technology, Karlsruhe, Germany
[b] Joint Research Laboratory Nanomaterials, Technische Universität Darmstadt and Karlsruhe Institute of Technology, Darmstadt, Germany
[c] Center for Functional Nanostructures, Karlsruhe Institute of Technology, Karlsruhe, Germany
[d] Helmholtz Institute Ulm for Electrochemical Energy Storage, Ulm, Germany
[e] Nonmetallic Inorganic Materials, ETH Zurich, Zurich, Switzerland

HIGHLIGHTS

- Nanocrystalline LSC was synthesized by salt-assisted spray pyrolysis method.
- Thin-film LSC cathodes were prepared by spin coating of stabilized dispersions.
- There is no need for sintering of the LSC thin films to obtain the desired phase.

ARTICLE INFO

Article history:
Received 5 July 2012
Received in revised form
7 November 2012
Accepted 29 November 2012
Available online 12 December 2012

Keywords:
Solid oxide fuel cell (SOFC)
Micro-SOFC
$La_{0.6}Sr_{0.4}CoO_{3-\delta}$ (LSC)
Thin film
Cathode
Salt-assisted spray pyrolysis

ABSTRACT

Nanocrystalline $La_{0.6}Sr_{0.4}CoO_{3-\delta}$ (LSC) powder with an ultrafine microstructure is synthesized via salt-assisted spray pyrolysis and subsequently stabilized in water-based dispersions. Nanoparticulate cathode thin films of LSC and LSC–GDC (gadolinium doped ceria) nanocomposites (with 10–40 wt% of GDC) are prepared via single step spin coating on yttria stabilized zirconia (YSZ) substrates. In order to prevent the chemical reaction between the cathode and the electrolyte, a thin buffer layer of GDC is deposited using spin coating on the YSZ substrates. The electrochemical performance of the thin film cathodes is measured by impedance spectroscopy on symmetrical cells in the temperature range of 450–650 °C. LSC cathode thin films (250 nm thick) with 30 wt% GDC content exhibit the lowest area specific resistance (ASR) values of 0.32, 0.78 and 2.04 Ω cm^2 in ambient air at 650, 600 and 550 °C, respectively.

1. Introduction

Solid oxide fuel cells (SOFCs) have been investigated extensively for the efficient and clean generation of electricity. Recently, micro-solid oxide fuel cells (micro-SOFCs) have drawn increasing attention as an alternative system for small-scale mobile power generation [1–14]. The high efficiency of micro-SOFCs and the utilization of high energy density fuels give rise to higher energy density power sources compared to conventional rechargeable Li-ion batteries [15]. Therefore, micro-SOFCs are anticipated to help satisfying the increasing energy demand for small portable electronic devices with low power requirements such as mobile phones, laptops and personal digital assistants [16]. In order to simplify thermal management in such devices, the operating temperature has to be reduced below 600 °C. In the past, a main strategy to reduce the operating temperature has been the use of thin-film solid electrolytes [17–19]. Thus, the ohmic losses are minimized within the cell by decreasing the length of the diffusion path of oxygen ions. Besides cutting down the ohmic resistance, the reduction of polarization losses at the electrodes can also facilitate lower operating temperatures. Therefore, alternative cathode materials with improved catalytic properties have been developed. Especially cathode materials with mixed ionic and electronic conductivity (MIEC) such as strontium doped lanthanum cobalt

* Corresponding author. Joint Research Laboratory Nanomaterials, Technische Universität Darmstadt and Karlsruhe Institute of Technology, Darmstadt, Germany. Tel.: +49 6151 16 75844; fax: +49 6151 16 6335.
E-mail address: cbenel@nano.tu-darmstadt.de (C. Benel).

0378-7753/$ – see front matter © 2012 Elsevier B.V. All rights reserved.
http://dx.doi.org/10.1016/j.jpowsour.2012.11.149

oxide ($La_{0.6}Sr_{0.4}CoO_{3-\delta}$) shows enhanced oxygen reduction kinetics compared to the conventional cathode material LSM ($La_{1-x}Sr_xMnO_{3\pm\delta}$) by providing an additional pathway through the bulk of the perovskite structure [20,21].

Several studies evidenced that oxygen reduction kinetics are governed by the oxygen exchange at the perovskite/air interface [22–25] for $La_{1-x}Sr_xCo_{1-y}Fe_yO_{3\pm\delta}$ electrodes. Thus the electrochemical performance may be enhanced either by increasing the electrode thickness [22] or by reducing the LSC grain size [23]. The second approach is favored in free-standing micro-SOFC for which the thickness has to be kept below 500 nm (typically) in order to maintain the thermomechanical stability of the cell [26].

Therefore, in order to enhance the electrode performance nanoparticles have been considered as their high surface area to volume ratio creates a large number of sites for oxygen exchange. Various solution-based methods such as sol–gel, precipitation and hydrothermal routes have been extensively investigated for the synthesis of nanoparticles. The major disadvantage of liquid-phase synthesis is the formation of hard agglomerates of the ultrafine particles [27], which leads to substantial reduction of the active surface area. As an alternative, several vacuum-based thin film deposition methods have been reported for the preparation of thin-film cathodes, such as pulsed laser deposition [21,28–32] and sputtering [5,33]. However, these methods are not cost-effective and not easy to scale up. From the application-oriented perspective, spray pyrolysis is a more versatile and inexpensive process for the synthesis of a variety of materials in various morphologies. In the conventional spray pyrolysis method, a solution of precursors is nebulized into droplets and continuously carried into a hot reaction zone where the decomposition of the precursors and the formation of the particles occur [34,35]. The final particle size depends on the initial precursor droplet size which is typically in the range from micrometer to sub-micrometer [34]. These particles are composed of nanocrystallites which are typically strongly agglomerated and which are, in most cases, practically inseparable. However, it has been recently reported that the utilization of inert inorganic salts in the precursor solutions leads to the fragmentation of agglomerated particles into much smaller nanoparticles [36–38]. This modified synthesis route is known as salt-assisted spray pyrolysis (SASP). This novel synthesis technique depends on the distribution of salt on the surfaces of the nanoparticles, which effectively prevents the agglomeration of the nanoparticles during the synthesis.

The aim of this study is to synthesize and investigate the structure and the electrochemical performance of LSC and LSC–GDC nanocomposite cathode thin ($\leq$500 nm) films based on agglomerate-free LSC nanoparticles synthesized via salt-assisted spray pyrolysis method. The electrodes were prepared by spin coating of stabilized nanodispersions and the electrochemical performance of symmetrical cells was evaluated using impedance spectroscopy.

2. Experimental

2.1. Salt-assisted spray pyrolysis of LSC nanopowder

The precursor solution is prepared from $La(NO_3)_2 \cdot 6H_2O$ (99.99%, Sigma–Aldrich Chemie GmbH, Steinheim, Germany), $Sr(NO_3)_2$ ($\geq$99%, Sigma–Aldrich Chemie GmbH, Steinheim, Germany) and $Co(NO_3)_2 \cdot 6H_2O$ ($\geq$98%, Sigma–Aldrich Chemie GmbH, Steinheim, Germany). The nitrates are dissolved in deionized water at room temperature to yield a total cation concentration of 0.05 M. The molar ratio of cations is adjusted to acquire the final composition of $La_{0.6}Sr_{0.4}CoO_{3-\delta}$. Sodium chloride (NaCl, $\geq$99.5%, Sigma–Aldrich Chemie GmbH, Steinheim, Germany) is added to the precursor solution as an inert inorganic salt. The concentration of NaCl in the precursor is adjusted to 1.0 M. The spray pyrolysis setup consists of a nebulizing chamber, a pyrolysis zone, and a powder collection chamber. In the nebulizing chamber, the precursor solution is in contact with a piezoelectric transducer and ultrasonically nebulized at 1.6 MHz. The misted precursor droplets are continuously carried into a hot tubular pyrolysis zone using oxygen flow rate of 5.0 l min^{-1}. The precursor feed rate is kept constant at 0.5 ml min^{-1}. The pyrolysis zone consists of an alumina tube placed in a three-zone tube furnace with a heated length of 120 cm. The nanoparticles are collected on a glass fiber filter placed in the collection chamber, which is held above 120 °C to eliminate water condensation. The pressure within the system is kept at 900 mbar by a vacuum pump and an automatically operating butterfly valve. The temperature of the first pyrolysis zone is held at 800 °C, which is the first heating zone of the tube furnace after the nebulizing chamber. The two following zones are kept at 750 °C. After the collection of the nanoparticles, NaCl in the as-synthesized powder is washed out thoroughly using deionized water by centrifuging.

2.2. Powder characterization

X-ray diffraction measurements (Bruker AXS D8 Advance, Karlsruhe, Germany) are carried out in Bragg–Brentano geometry using CuK_α radiation with an energy dispersive detector (Bruker AXS, Sol-X) from 15° to 85° with a step size of 0.02° and a scan rate of 5 s $step^{-1}$. The XRD patterns are analyzed by Rietveld refinement using the software of Topas 3.0 (Bruker AXS, Karlsruhe, Germany).

The microstructure of the samples is investigated by high-resolution scanning electron microscopy (HRSEM) using a Philips XL30 FEG. Gold-palladium is sputtered onto the samples to prevent electrical charging. The specific surface area of the as-prepared powder is determined by nitrogen adsorption measurements using a Quantachrome Autosorb-3b instrument (Quantachrome, Boynton Beath, FL). Each sample is degassed for 24 h at 150 °C in vacuum prior to the measurement. The isotherms are analyzed using the BET method [39].

2.3. Preparation of stabilized dispersions of LSC and LSC–GDC nanocomposites

To prepare stabilized dispersions of LSC, the washed powder is dispersed in an aqueous NH_3 solution (pH = 10) and sonicated for 30 s using a compact ultrasonic laboratory device (Hielscher UP400H, Teltow, Germany). For further stabilization of the dispersions, the polyalcohol-based stabilizer KX9009 (Zschimmer & Schwarz GmbH, Lahnstein, Germany) is used. Nanocomposite dispersions of LSC–GDC (10–40 wt%) are prepared by adding commercial GDC nanopowder (Ceria-20 wt% gadolinium, 100 $m^2 g^{-1}$, Sigma–Aldrich, Steinheim, Germany) to the stabilized LSC dispersions followed by 30 s sonication of the dispersion to ensure homogeneous mixing. Zeta potential measurements of the stabilized dispersions of the LSC and GDC nanopowders are performed using a ZetaSizer Nano SZ (Malvern Instrument, Worcestershire, UK).

2.4. Thin film preparation and electrochemical characterization

For the electrochemical characterization, cathode thin films of LSC and LSC–GDC nanocomposite are prepared using spin coating. A symmetrical geometry on polycrystalline YSZ substrates (200 μm thickness, 8 mol% yttria, Itochu, Japan) was employed. In order to avoid chemical reactions between LSC and YSZ, GDC thin films are deposited as a buffer layer by spin coating of the stabilized GDC dispersion prior to the deposition of the active cathode layers. Subsequently, the GDC/YSZ/GDC samples are heat treated at 950 °C for 2 h. The LSC and LSC–GDC (10–40 wt%) cathode thin films with

thicknesses of about 250 nm and 500 nm are deposited symmetrically on the GDC/YSZ/GDC substrates by spin coating of stabilized dispersions, followed by sintering at 550 °C for 1 h to obtain good connectivity between the nanoparticles within the cathode layers. As a current collector layer, a commercial LSM ($(La_{0.8}Sr_{0.2})_{0.95}MnO_3$) paste (mean particle size of d_{50} = 0.39 μm, specific surface area of 4.66 m^2 g^{-1}, Nextech Materials, Lewis Center, OH) is screen-printed (mesh 325) symmetrically on each sample. The thickness of the porous current collector layer is determined to be 10 μm from cross-sectional HRSEM micrographs. Subsequent to screen printing, the current collector layers are dried for 12 h at 80 °C.

The electrochemical characterization of the symmetrical cells is conducted via Electrochemical Impedance Spectroscopy (EIS) by using a Solartron 1260 frequency response analyzer. The impedance measurements are performed at electrochemical equilibrium (zero DC bias) by applying an AC signal with 20 mV amplitude over a frequency range of 0.05 Hz–1 MHz. Each sample is measured in the temperature range from 650 °C to 450 °C with steps of 50 °C. All impedance measurements are acquired after the temperature of the sample is stabilized. The sample is positioned between two alumina pieces. The contact sides of the alumina pieces are slotted to allow proper gas access to the sample. Platinum gauze (mesh 100) is used as a metallic electrode and two platinum wires are spot-welded on each gauze to serve as current and voltage probes. The proper contact between the sample and platinum gauzes is achieved by the weight of an alumina block. The impedance spectra are analyzed by using ZView 2.90 (Scribner Associates, Inc.).

3. Results and discussion

3.1. Microstructure and XRD analyses

Fig. 1a shows the typical hollow sphere morphology of as-synthesized LSC powder obtained by citric acid assisted spray pyrolysis [40,41]. The powder consists of hollow spheres with diameters in the range of 0.5–5 μm and very thin shells. Even though the hollow spheres are in micron size in diameter, they consist of thin shells comprising nanocrystallites and it is expected that the shells can be easily broken into very fine initial nanoparticles. Nevertheless, attempts to improve the morphology by application of ultrasonic energy have not been sufficient in case of LSC and the shells are not broken up completely into the primary nanoparticles, as seen in Fig. 1b. On the other hand, Fig. 1c shows the typical morphology of as-synthesized LSC powder

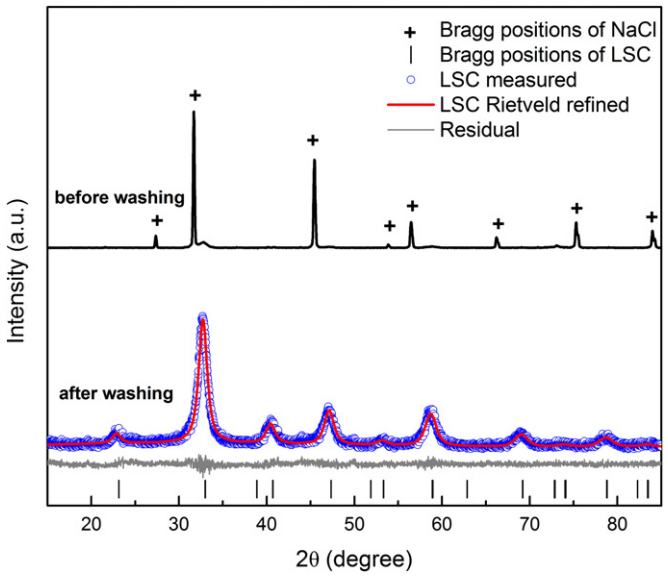

Fig. 2. X-ray diffraction patterns of LSC nanoparticles before and after washing of NaCl and Rietveld refinement for washed LSC nanopowder.

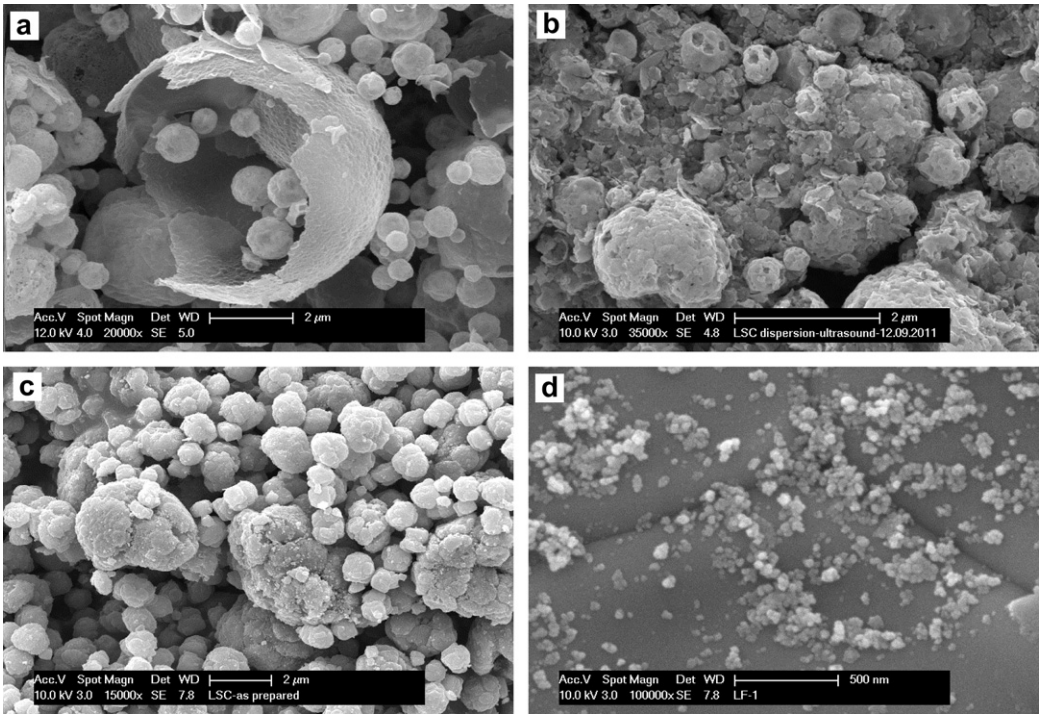

Fig. 1. Scanning electron micrographs of (a) as-synthesized LSC powder prepared by citric acid assisted spray pyrolysis, (b) LSC powder after ultrasonication, (c) as-synthesized LSC powder prepared by salt assisted spray pyrolysis, and (d) LSC powder after washing.

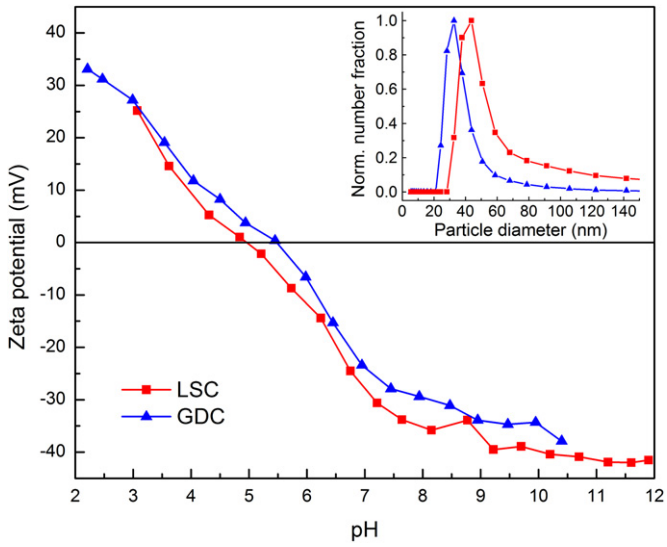

Fig. 3. Zeta potential and particle size distribution (inset) of LSC and GDC nanoparticles.

obtained by salt assisted spray pyrolysis. Instead of the hollow sphere morphology, as-synthesized powders reveal a collapsed agglomerated sphere morphology. As it is confirmed in Fig. 1d, the removal of salt by washing of the as-synthesized powder leads to an improvement of the morphology by a reduction of the degree of agglomeration. The salt (NaCl) phase within the powder behaves as a filler to prevent the further agglomeration and sintering of the individual nanoparticles [42]. Therefore, as-synthesized powder can be used immediately after washing as a raw material for functional cathode layers.

XRD patterns of LSC powders before and after washing are shown in Fig. 2. As-synthesized powder consists to a large fraction of NaCl, but without any indication of a reaction between LSC and NaCl. From the XRD patterns of washed powder, it is evident that NaCl is completely removed from the system by the chosen procedure. The Rietveld refinement of XRD pattern (ICSD #82817) of washed LSC powder indicates the formation of a nanocrystalline single-phase perovskite structure. Atomic absorption spectroscopy (AAS) measurements of the washed LSC powder verify the complete removal of NaCl. The average crystallite size is calculated to be approximately 7 nm from the refinement. The specific surface areas of the LSC powders obtained from salt-assisted (washed powder) and non-salt-assisted spray pyrolysis methods under the same synthesis conditions are found to be 60 $m^2\ g^{-1}$ and 39 $m^2\ g^{-1}$, respectively. It is observed that salt-assisted synthesis of LSC nanoparticles leads to a surface area enhancement of 50%.

3.2. Characterization of dispersions

Zeta potential measurements are performed to predict the stability of the dispersions of LSC and GDC nanoparticles. Fig. 3 shows the zeta potential as a function of pH of the aqueous LSC and GDC dispersions. The Zeta potential curves for both materials indicate that the nanoparticles have the highest degree of dispersion stability at pH values in the range of approximately 9–12 since the Zeta potential measurements show values greater than 30 mV (absolute value). Based on this result, the electrosteric stabilization mechanism (combination of electrostatic and steric stabilizations) is employed to control the stability of the dispersions. For further experiments using spin coating, the nanoparticles were dispersed at pH = 10. Particle size distribution measured at pH = 10 (Fig. 3, inset) shows the medium particle diameter of 44 nm and 33 nm for LSC and GDC nanoparticles, respectively.

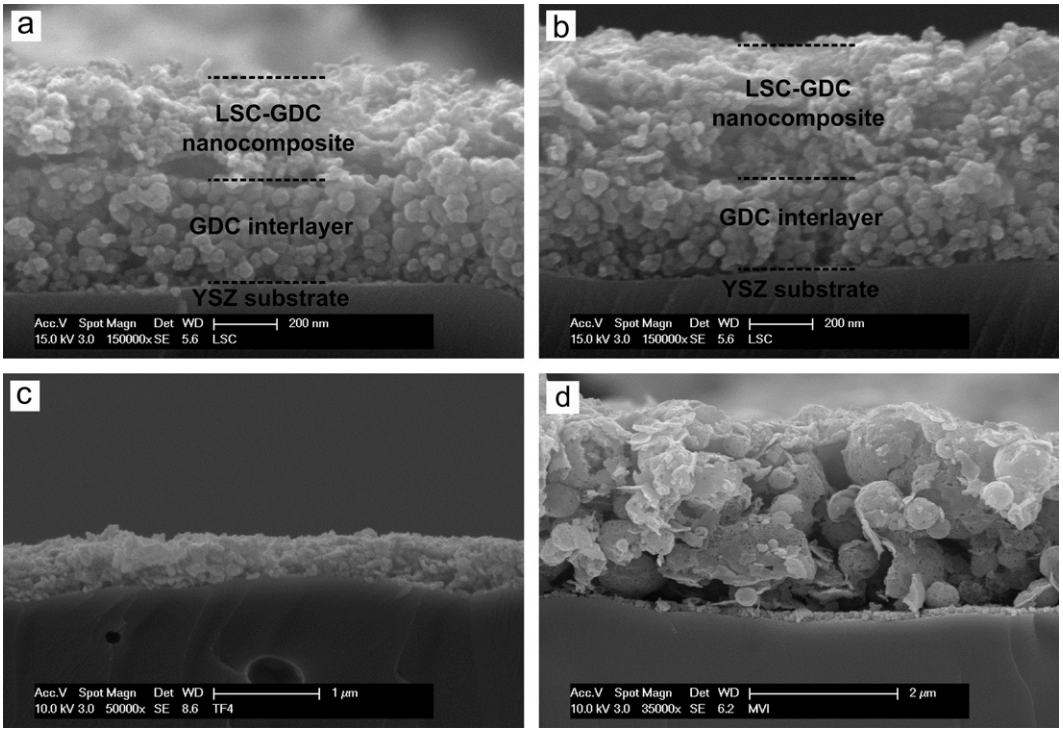

Fig. 4. Scanning electron micrographs (a) and (b) of cross-sections of LSC–GDC nanocomposite functional layers (obtained from salt-assisted spray pyrolysis method) with different thicknesses coated on YSZ substrate with a GDC interlayer, (c) of LSC functional layer (obtained from salt-assisted spray pyrolysis method) on YSZ substrate without GDC interlayer, and (d) of LSC functional layer obtained from non-salt-assisted spray pyrolysis method.

3.3. Electrode fabrication and electrochemical characterization

The scanning electron micrographs in Fig. 4a–c shows the cross-section of spin coated LSC (Fig. 4c) and LSC–GDC nanocomposite (Fig. 4a, b) functional layers with thicknesses between 250 and 500 nm, which are obtained from salt-assisted spray pyrolysis method. It is evident that both functional cathode layers and GDC interlayers are continuous and homogeneous in thickness and that proper contact between the layers has been achieved. The thickness of the LSC functional layer can be controlled within the range of 150–500 nm by adjusting the concentration of the dispersion and the parameters of the spin coating. The thickness of GDC interlayer is set to approximately 300 nm. The SEM image in Fig. 4d shows the cross-section of the spin coated LSC functional layer which is derived from non-salt-assisted spray pyrolysis method. The layers are not appropriate for thin film SOFC, since they consist of hollow spheres with diameters in the range of 0.5–5 μm, which exhibit strong agglomeration. Since the attempts to improve the morphology of the starting LSC powder by the application of ultrasonic energy are not successful, thin film processing from such samples (Fig. 4d) lead to thick and inhomogeneous LSC functional layers.

Fig. 5 shows representative impedance spectra in the form of a Nyquist plot obtained from a symmetrical cell with the layers of LSC-30%GDC/GDC/YSZ/GDC/LSC-30%GDC measured in the temperature range of 450–650 °C. It is observed that the impedance spectra consist of three contributions: series of resistance accounting for the current collection and ohmic losses in the cell, high frequency arc originating from the electrolyte, and low frequency depressed semi-circle which is typical for the oxygen reduction at porous mixed ionic electronic electrodes such as LSC [20].

Fig. 6a shows the temperature dependence of oxygen reduction ASR for pure LSC and LSC–GDC (10–40 wt%) composite cathodes. A good linearity between the ASR of cathode and the reciprocal temperature is obtained in the temperature range of 450–650 °C. The decrease of ASR upon increasing the thickness proves that oxygen exchange at the perovskite–air interface is indeed a rate-determining step of the oxygen reduction reaction. The activation energies of 1.42 ± 0.03 eV and 1.41 ± 0.05 eV are calculated for the pure LSC cathode layers with thicknesses of 250 and 500 nm, respectively, which is in good agreement with the activation energies of 1.41 eV for $La_{0.6}Sr_{0.4}CoO_{3-\delta}$ thin films obtained by metal organic deposition [23], 1.40 eV [21] and 1.52 [43] for $La_{0.6}Sr_{0.4}CoO_{3-\delta}$ thin films by PLD. The activation energies of 1.13 ± 0.06, 1.07 ± 0.03, 1.22 ± 0.03 and 1.19 ± 0.02 eV are determined for the LSC–GDC nanocomposite cathode layers for 10, 20, 30 and 40 wt% GDC concentrations, respectively. In Table 1, the ASR value obtained in this work is compared to those reported in the literature for thin porous LSC electrodes with similar microstructures. It appears that a trend exists between grain size and ASR. Smaller grain sizes lead to electrodes with higher pore wall surface area for oxygen exchange.

Fig. 6b emphasizes the evolution of the change in ASR values with respect to the fraction of GDC. It is apparent that the addition of GDC nanoparticles into the LSC nanostructure enhances the

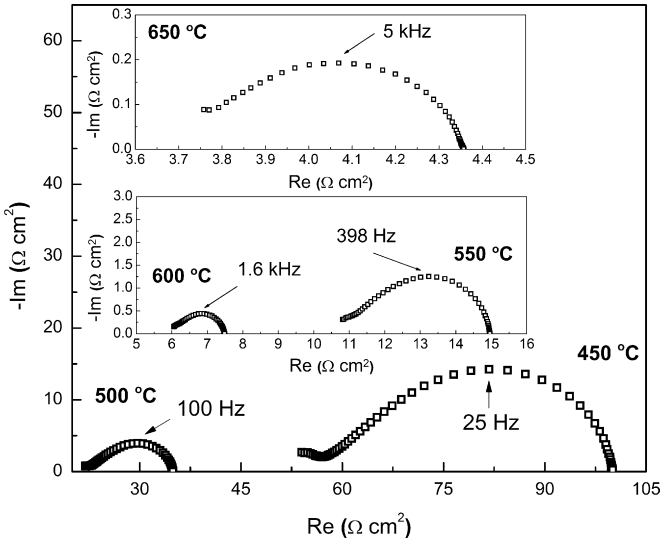

Fig. 5. Representative impedance spectra of a symmetrical cell with nanocomposite cathode thin film of LSC-30 wt% GDC measured in the temperature range of 450–650 °C in air.

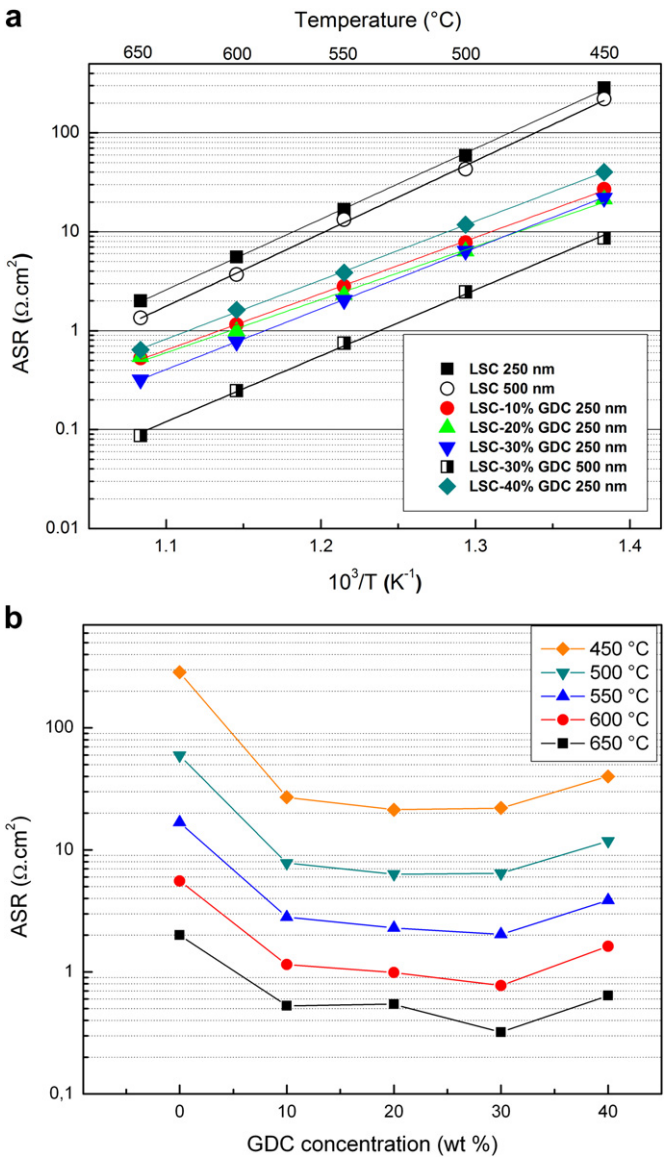

Fig. 6. The two graphs depict (a) dependence of area specific resistance (ASR) on operating temperature for LSC and LSC–GDC composite cathode thin films and (b) dependence of area specific resistance (ASR) on GDC content at different operating temperatures.

Table 1
Area specific resistance (ASR) values of LSC thin film cathodes prepared by different deposition methods.

Cathode material	ASR (Ω cm^2) at 600 °C	Deposition method	Thickness (nm)	Grain size (nm)	Reference
$La_{0.6}Sr_{0.4}CoO_{3-\delta}$	5.54	Spin coating	250	44	This work
$La_{0.6}Sr_{0.4}CoO_{3-\delta}$	0.96	Flame spray deposition	200	34	[43]
$La_{0.6}Sr_{0.4}CoO_{3-\delta}$	0.023	Metal organic deposition	200	17	[23]

electrochemical performance of the cathode functional layers. A similar approach to improve electrochemical activity of LSC cathode layers has also been reported [44,45]. However, further increase of GDC content in LSC leads to higher polarization losses. The similar trend between the ASR and the GDC composition for the same material system has been reported by Tao et al. [44]. It is not the scope of this paper to discuss in detail the oxygen reduction mechanism and kinetics of complex composite structure involving mixed ionic electronic conductors, yet the lower ASR values for LSC–GDC nanocomposite cathodes may indicate that introduction of GDC nanoparticles enhances the reaction kinetics by creating triple phase boundary (LSC/GDC/air) at which the oxygen could be reduced in parallel to the pathway through the bulk of the LSC.

4. Conclusion

In this work, the applicability of salt-assisted spray pyrolysis for the synthesis of nanocrystalline LSC cathode materials characterized by a low degree of agglomeration is successfully demonstrated. Microstructural characterization reveals that the morphology of the as-synthesized powder is improved significantly after the removal of salt without the need of further processing compared to nanopowders synthesized through conventional spray pyrolysis methods. Thin film cathodes (250 nm) of pure LSC and LSC–GDC nanocomposites (10–40 wt%) suitable for micro-SOFC applications are prepared by a single-step spin-coating of stabilized dispersions. The thickness of LSC functional layer is controlled within the range of 150–500 nm by adjusting the dispersion concentration and spin coating parameters. As one of the major advantages of the proposed method, it should be mentioned that there is no need for high temperature sintering of the thin films to obtain the desired LSC phase. The novel method offers an inexpensive, versatile and easily scalable thin film processing method compared to conventional vacuum based thin film fabrication techniques, such as PLD and CVD. Electrochemical characterization shows that introduction of GDC nanoparticles into the LSC nanostructure enhances the cathode activity.

The future work will focus on detailed chemical and microstructural analysis of the nanoparticulate LSC and LSC–GDC thin film cathodes to gain more understanding on the electrochemical processes within the functional layers. The synthesis method will be modified to obtain LSC nanoparticles with smaller grain size, which can improve the electrochemical performance of the LSC electrodes. Furthermore, long-term stability and degradation of the material will be investigated.

Acknowledgment

This work is supported by the German Research Foundation (Deutsche Forschungsgemeinschaft–DFG) and the State of Baden-Württemberg through the Center for Functional Nanostructures (CFN) within the sub-project F2.6. One of the authors (HH) is grateful for an equipment grant by the State of Hesse for the KIT-TUD Joint Research Laboratory Nanomaterials at Technische Universität Darmstadt. ETHZ acknowledges the financial support of the Swiss National Science Foundation (contract CRSI22-126830).

References

[1] A. Evans, A. Bieberle-Hütter, J.L.M. Rupp, L.J. Gauckler, J. Power Sources 194 (2009) 119.
[2] A. Evans, M. Prestat, R. Tölke, M.V.F. Schlupp, L.J. Gauckler, Y. Safa, T. Hocker, J. Courbat, D. Briand, N. de Rooij, D. Courty, Fuel Cells 12 (2012) 614.
[3] M.V.F. Schlupp, M. Prestat, J. Martynczuk, J.L.M. Rupp, A. Bieberle-Hütter, L.J. Gauckler, J. Power Sources 202 (2012) 47.
[4] H. Huang, M. Nakamura, P.C. Su, R. Fasching, Y. Saito, F.B. Prinz, J. Electrochem. Soc. 154 (2007) B20.
[5] B. Lai, K. Kerman, S. Ramanathan, J. Power Sources 195 (2010) 5185.
[6] I. Garbayo, A. Tarancon, J. Santiso, F. Peiro, E. Alarcon-Llado, A. Cavallaro, I. Gracia, C. Cane, N. Sabate, Solid State Ionics 181 (2010) 322.
[7] J.H. Shim, J.S. Park, J. An, T.M. Gür, S. Kang, F.B. Prinz, Chem. Mater. 21 (2009) 3290.
[8] C. Kwon, J. Son, J. Lee, H. Kim, H. Lee, K. Kim, Adv. Funct. Mater. 21 (2011) 1154.
[9] P. Su, C. Chao, J.H. Shim, R. Fasching, F.B. Prinz, Nano Lett. 8 (2008) 2289.
[10] A. Evans, S. Karalić, J. Martynczuk, M. Prestat, R. Tölke, L.J. Gauckler, ECS Trans. 45 (2012) 475.
[11] S. Rey-Mermet, Y. Yan, C. Sandu, G. Deng, P. Muralt, Thin Solid Films 518 (2010) 4743.
[12] J.S. Park, Y.b. Kim, J.H. Shim, S. Kang, T.M. Gür, F.B. Prinz, Chem. Mater. 22 (2010) 5366.
[13] M. Prestat, A. Evans, R. Tölke, M.V.F. Schlupp, B. Scherrer, Z. Yáng, J. Martynczuk, O. Pecho, H. Ma, A. Bieberle-Hütter, L.J. Gauckler, Y. Safa, T. Hocker, L. Holzer, P. Muralt, Y. Yan, J. Courbat, D. Briand, N.F. de Rooij, Proceedings of the 10th European. Fuel Cell Forum, F. Lefebvre-Joud et al. (Eds.), Lucerne, Switzerland, 2012, p. A07–A30.
[14] B. Scherrer, A. Rossi, J. Martynczuk, M.D. Rossell, A. Bieberle-Hütter, J.L.M. Rupp, R. Erni, L.J. Gauckler, J. Power Sources 196 (2011) 7372.
[15] G.J. La O, H.J. In, E. Crumlin, G. Barbastathis, Y. Shao-Horn, Int. J. Energy Res. 31 (2007) 548.
[16] A. Bieberle-Hutter, D. Beckel, A. Infortuna, U.P. Muecke, J.L.M. Rupp, L.J. Gauckler, S. Rey-Mermet, P. Muralt, N.R. Bieri, N. Hotz, M.J. Stutz, D. Poulikakos, P. Heeb, P. Muller, A. Bernard, R. Gmur, T. Hocker, J. Power Sources 177 (2008) 123.
[17] J. Seydel, M. Becker, E. Ivers-Tiffee, H. Hahn, Mater. Sci. Eng. B 164 (2009) 60–64.
[18] D. Beckel, A. Bieberle-Hutter, A. Harvey, A. Infortuna, U.P. Muecke, M. Prestat, J.L.M. Rupp, L.J. Gauckler, J. Power Sources 173 (2007) 325–345.
[19] B.C.H. Steele, A. Heinzel, Nature 414 (2001) 345–352.
[20] S.B. Adler, Chem. Rev. 104 (2004) 4791–4843.
[21] J. Januschewsky, M. Ahrens, A. Opitz, F. Kubel, J. Fleig, Adv. Funct. Mater. 19 (2009) 3151–3156.
[22] H.-S. Noh, H. Lee, H.-I. Ji, H.-W. Lee, J.-H. Lee, J.W. Son, J. Electrochem. Soc. 158 (2011) B1–B4.
[23] J. Hayd, L. Dieterle, U. Guntow, D. Gerthsen, E. Ivers-Tiffee, J. Power Sources 196 (2011) 7263–7270.
[24] F.S. Baumann, J. Fleig, H.-U. Habermeier, J. Maier, Solid State Ionics 177 (2006) 1071–1081.
[25] E. Mutoro, E.J. Crumlin, M.D. Biegalski, H.M. Christen, Y. Shao-Horn, Energy Environ. Sci. 4 (2011) 3689–3696.
[26] A. Evans, PhD thesis, ETH Zurich (2012), A. Evans, PhD thesis, ETH Zurich (2012), http://dx.doi.org/10.3929/ethz-a-007339508
[27] J.G. Li, T. Ikegami, J.H. Lee, T. Mori, Acta Mater. 49 (2001) 419–426.
[28] X. Chen, S. Wang, Y.L. Yang, L. Smith, N.J. Wu, B.-I. Kim, S.S. Perry, A.J. Jacobson, A. Ignatiev, Solid State Ionics 146 (2002) 405–413.
[29] D. Mori, H. Oka, Y. Suzuki, N. Sonoyama, A. Yamada, R. Kanno, Y. Sumiya, N. Imanishi, Y. Takeda, Solid State Ionics 177 (2006) 535–540.
[30] E. Koep, C. Jin, M. Haluska, R. Das, R. Narayan, K. Sandhage, R. Snyder, M. Liu, J. Power Sources 161 (2006) 250–255.
[31] M. Prestat, A. Infortuna, S. Korrodi, S. Rey-Mermet, P. Muralt, L.J. Gauckler, J. Electrochem. Soc. 18 (2007) 111.
[32] P. Plonczak, M. Sogaard, A. Bieberle-Hütter, P.V. Hendriksen, L.J. Gauckler, J. Electrochem. Soc. 159 (2012) 471–482.
[33] A.C. Johnson, B.-K. Lai, H. Xiong, S. Ramanathan, J. Power Sources 186 (2009) 252–260.
[34] G.L. Messing, S.C. Zhang, G.V. Jayanthi, J. Am. Ceram. Soc. 76 (1993) 2707–2724.
[35] I.W. Lenggoro, T. Hata, F. Iskandar, M.M. Lunden, K. Okuyama, J. Mater. Res. 15 (2000) 733–743.
[36] B. Xia, I.W. Lenggoro, K. Okuyama, J. Mater. Chem. 11 (2001) 2925–2927.
[37] B. Xia, I.W. Lenggoro, K. Okuyama, Adv. Mater. 13 (2001) 1579–1582.
[38] B. Xia, I.W. Lenggoro, K. Okuyama, Chem. Mater. 14 (2002) 2623–2627.

[39] S. Brunauer, P.H. Emmett, E. Teller, J. Am. Chem. Soc. 60 (1938) 309.
[40] A.J. Darbandi, H. Hahn, Solid State Ionics 180 (2009) 1379–1387.
[41] A.J. Darbandi, T. Enz, H. Hahn, Solid State Ionics 180 (2009) 424–430.
[42] S.G. Lee, S.M. Choi, D. Lee, Thermochim. Acta 455 (2007) 138–147.
[43] N.I. Karageorgakis, A. Heel, A. Bieberle-Hutter, J.L.M. Rupp, T. Graule, L.J. Gauckler, J. Power Sources 195 (2010) 8152–8161.
[44] Y. Tao, J. Shao, W.G. Wang, J. Wang, Fuel Cells 5 (2009) 679–683.
[45] H. Nie, S. Wang, Z. Wang, J. Qian, T.-L. Wen, Solid State Ionics 192 (2011) 483–485.